Volume Visualization in Cell Biology

A. Kaufman, R. Yagel, R. Bakalash
Department of Computer Science

I. Spector
Department of Physiology & Biophysics

State University of New York at Stony Brook
Stony Brook, NY 11794

Abstract

Living cells are 3D objects with a complex inner structural organization. Understanding this organization and its relation to biological function constitutes a major challenge for cell biologists. This paper discusses the special properties of volumetric cell data (e.g., noise, discontinuity, raggedness) and the particular difficulties encountered when trying to visualize them in 3D. We describe some of the solutions we adopted, specifically in surface discrimination and shading. These solutions have been implemented as an integral part of the BioCube system, an environment for volume visualization of cellular structures. The paper presents volume visualization results for the actin cytoskeleton of single cells.

Key Words: volume rendering, biological visualization, discrete shading, cytoskeleton

Introduction

The mechanisms by which various types of cells acquire and maintain their distinctive shapes are fundamental problems of cell biology. Actin-microfilament proteins, a major component of the cell skeleton (cytoskeleton), participate in the determination of the cell shape and in a range of cell motility phenomena such as cell division and crawling of cells on a substratum. Traditional light microscopy techniques (e.g., phase contrast, differential interference contrast) do not allow the identification of cytoskeletal proteins (see Figure 1). The advent of specific fluorescent labeling probes for actin have eased the task of cytoskeleton visualization by providing the means to dye these subcellular structures and observe them by fluorescence microscopy. However, both light and fluorescence microscopy provide the biologist with 2D images that can be viewed clearly only if the specimen under study is in the focal plane. This is why biologists have tended to examine flat specimens, which do not have too much out-of-focus information, at the expense of thicker specimens, which are degraded by unwanted information projected from adjacent focal planes (see Figure 2).

To overcome the severe limitations of these 2D visualization techniques, novel microscopic technologies have been developed. These include confocal microscopy [18] and optical serial sectioning microscopy [1, 4] which are capable of producing a sequence of 2D in-focus cross sections of biological specimens. These cross sections can then be viewed as a sequence of images without the out-of-focus information, or they can be integrated into a high resolution 2D image similar to the one acquired by a light microscope but without the out-of-focus information (see Figure 3).

Ideally, however, the slices can be utilized to reconstruct a 3D volumetric dataset. The internal or external parts of this dataset can be examined and manipulated through the application of volume rendering techniques, which provide the biologist with views of the cell not possible by direct viewing with the microscope. This task may seem simple considering the body of information that already exists in the case of volume visualization of medical applications. Researchers using CT or MRI data of human organs have developed algorithms for data enhancement, interpolation [20], surface tracking and detection [2, 17], projection [6, 16, 26], and shading [3, 7, 10]. While these methods have matured enough to be used in real clinical applications with data obtained from CT or MRI of human organs (e.g., [19, 21, 24, 28]), the biological case poses special difficulties.

CH2913-2/90/0000/0160/$01.00 – 1990 IEEE

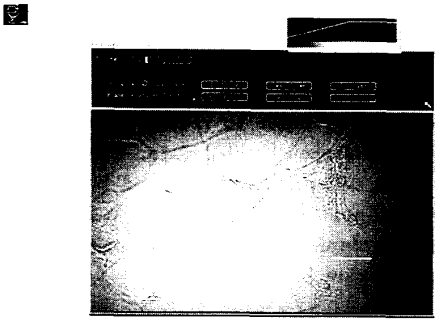

Figure 1: Appearance of cells of neuroblastoma clone N1E-115 as viewed by bright field optics. A large cell bearing numerous processes is shown in the middle of the micrograph. The circular shape at the cell center is the cell nucleus. Calibration bar is 25μm .
(Color Plate 67, page 471)

Figure 2: Micrograph showing the organization of actin structures in N1E-115 cells. The cells were stained with rhodamine-phalloidin a fluorescent toxin which bind specifically to actin filaments, and viewed in a conventional fluorescence microscope. Notice the blurry areas caused by the out-of-focus light contribution in thick cell areas.
(Color Plate 68, page 471)

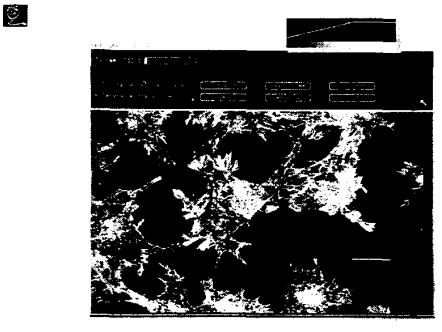

Figure 3: Rhodamine-phalloidin staining of N1E-115 cells viewed in a fluorescence confocal microscope. Image of actin structures is created by integrating 60 slices. Calibration bar is 25μm . **(Color Plate 69, page 471)**

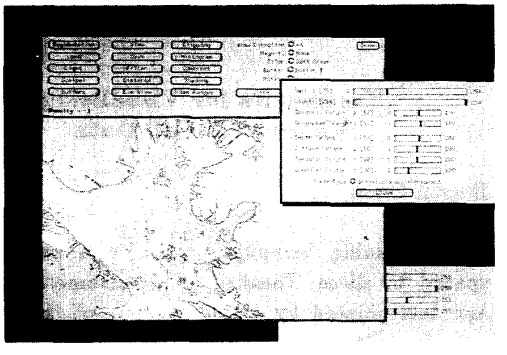

Figure 4: Volume rendering of actin structures of the cell shown in the center of Figures 1 and 3. A nerve process that extends to the left was clipped. **(Color Plate 70, page 471)**

The application of the methods devised for medical visualization to our biological datasets proved to be inadequate or inefficient. Compared to volume data found in medical applications, biological datasets have diverse and changing morphologies. They tend to be noisier, have ragged contours, have many disconnected objects with irregular features, and are greatly non-isometric. These characteristics require the design of special solutions. Previous research in this field has utilized simple visualization tools such as stereoscopy, depth-only shading where the object's shade is determined solely by its distance from the observer, or animation of unshaded projections where the sense of depth is achieved mainly by motion parallax [1, 4, 27].

In this paper we discuss the inherent difficulties encountered in visualizing datasets from fluorescence confocal microscopy and some of the solutions we have adopted. We have chosen nerve cells (neuroblastoma) grown in tissue culture as our biological preparation because these cells possess very rich actin structures. The cells were stained with a fluorescent probe specific for actin (rhodamine-phalloidin) [25]. They were viewed and optically sectioned using the Bio-Rad MRC 600 confocal fluorescence microscope. The slice dataset was then reconstructed and processed in the BioCube environment – a comprehensive system that we have developed for volume visualization of cellular structures. The actin cytoskeleton of single cells was visualized and manipulated using this system.

Techniques for Visualizing Volumetric Cell Data

Depth Cues

Most scanning techniques produce a sequence of spaced 2D slices. These slices are commonly stacked and interpolated by employing one of the nearest-neighbor, linear, or cubic interpolation techniques, complemented with noise reduction tools. The volumetric data can then be stored and retrieved from an archival storage system which supports several volume representations (e.g., 3D array, runlength compression, voxel list).

In contrast to most specimens used in medicine which provide sufficient information in all three dimensions, cells are small and rather flat, and may exhibit a ratio of 1 to 30 between the Z and the X-Y dimensions. Thus, the perception of depth and the production of shading-based depth cues are extremely difficult. The solution we adopted is to exaggerate the Z dimension by inserting additional slices between the original ones. The insertion of slices is done by first (linear) or higher order (e.g., cubic) interpolation, and not by zero order (slice duplication), in order to reduce the appearance of jaggies in the reconstructed data. Figure 4 shows an image of a cell originally acquired in $512 \times 768 \times 60$ that was clipped and interpolated to $256 \times 256 \times 180$. It depicts volume rendering of the cell located at the center of Figure 1.

Another mechanism that enhances depth understanding is the interactive and dynamic positioning of the light source. This is achieved by utilizing the congradient shading technique [3], which is a table-driven, hardware-oriented shading method that operates in pixel space. This technique supports real-time image updates simply by using a new pre-computed lookup table every time the shading parameters (such as light-source location, color, or intensity) change.

One of the most effective depth cues is achieved by providing the observer with an animation sequence of parallel projections. However, the usefulness of this method is limited since the biologist can extract significant information by carefully examining a well-shaded still image rather than watching a spinning object.

Surface Discrimination

Biological datasets differ from medical datasets in several aspects. Biological datasets tend to be noisier, thus it is necessary to apply image enhancement operations on both the 2D slice images as well as on the 3D reconstructed volume. Figure 5 presents a left side view of the cell shown in Figure 4, where a noisy slice can be noticed. In contrast to the relatively smooth and well-defined boundaries of bodily organs, single cells are characterized by a complex network of surface protrusions making their contours extremely ragged (see Figures 4 and 5). In

addition, while medical datasets tend to contain few continuous objects, biological images might have numerous disconnected small objects. Thus, algorithms routinely used for medical datasets that rely on user intervention (e.g., manual contour tracking, seed picking on surfaces) would require a prohibitive amount of user labor in the case of the biological datasets.

As alternatives, we have implemented two surface extraction algorithms that overcome the three problems of noisiness, raggedness, and discontinuity. The first method requires the user to pick one seed point in the background, which is used by a recursive scan-line based flooding algorithm to detect the entire background. This flooding algorithm is a 3D extension of the 2D flooding algorithm [5]. Once the background has been detected, the outer surface of all objects in the volume can be extracted easily since it is simply the set of all voxels that are adjacent to the background voxels.

The second algorithm for surface discrimination adopts a non-recursive slice-oriented approach to provide a fully automatic surface extraction capability. In each slice, rays parallel to the axis scan the slice and identify all possible seeds, eliminating the need for user intervention. These seeds are then used as input for a 2D contour extraction mechanism, which detects all contours in a given slice that are visible from an orthographic viewing direction. Repeating this seed detection and contour extraction process three times (for the three axes) yields a set of voxels that approximates the set of all possibly visible voxels [24].

Shading

One of the severe problems we have encountered with our biological datasets is the poor performance of existing shading methods. Specifically, the following three techniques have been investigated: congradient shading [3] (a variation of depth gradient shading [7]), where surface inclination at a specific pixel is estimated from the relative depth of its adjacent neighbors; grey-level shading [10], where surface inclination is estimated from the value (grey level) of voxel's neighbors; and depth-only shading (e.g., [8]), where the color of an object is determined solely by its distance from the observer.

Since the scene in our datasets is commonly composed of many disconnected small objects and is speckled with noise, pixel space shading methods (e.g., depth-gradient and congradient shading) would fail. Voxel space shading methods (e.g., grey-level gradient) would fail because many objects are thin and have a ragged boundary. Depth-only shading will smooth the sampling noise, but this method would fail because it suppresses the minute details that are essential in our application. The first solution we have developed is to blend, for each pixel, the colors calculated by several shading methods. The exact weight given to each method in the final color is user controllable and can be tuned to achieve the best results. More formally, the final pixel intensity $\bar{I}$ is computed as a linear combination of the three methods:

$$\bar{I} = k_d I_d + k_c I_c + k_g I_g \qquad (1)$$

where I_d, I_c, I_g are the intensities for a specific pixel calculated by the depth-only, congradient, and grey-level methods, respectively, and k_d, k_c, k_g are the respective weights chosen by the user (such that $k_d + k_c + k_g = 1$). Figures 4-7 show images shaded with such a combination.

This solution, however, brings only a partial remedy to the shading problem. We have observed that the use of information from a small and fixed neighborhood, coupled with the inability to detect surface and inclination discontinuities, accounts for most maladies encountered in the existing shading methods. Based on these observations, a method called *context sensitive* shading has been designed. This method employs a mechanism for discontinuity detection, which segments the image space into *contexts*, each of which is a surface segment that exhibits a high level of uniformity. That is, a context is a continuous surface (C^0-continuity) with a gradually changing tangent (C^1-continuity). Successive operations aiming at gradient estimation are all restricted to the information available in one context, making them *context sensitive*. Context sensitive prefiltering and postfiltering are also suggested as remedies for the sensitivity to noise and discretization artifacts [29]. It should be noted that segmentation into contexts, context sensitive operators, and gradient estimation can be implemented in both voxel space or pixel space. We have chosen to implement a pixel-based version of

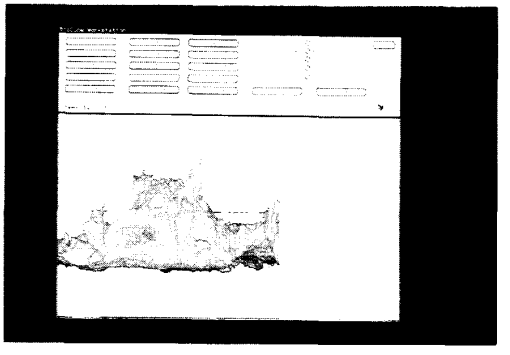

Figure 5: A side view of the same cell shown in Figure 4, exposing the cut in the nerve process. This demonstrates that the central core of the process is devoid of actin. **(Color Plate 71, page 471)**

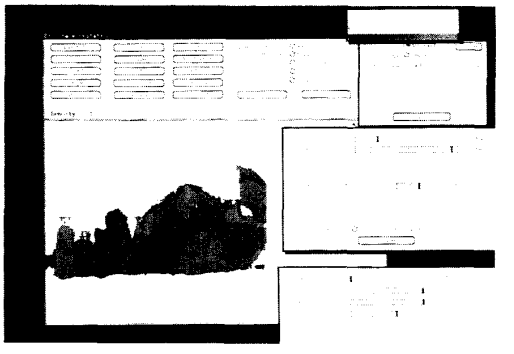

Figure 6: A side view of the interior of the cell cut vertically through the nuclear region. The cut exposes a hollow part in the area where the nucleus resides. The visible surface protrusions are highly dynamic motile structures.
(Color Plate 72, page 471)

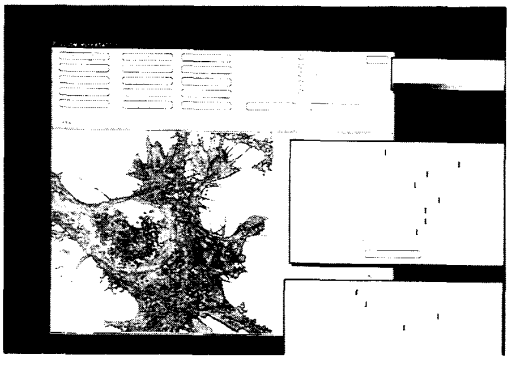

Figure 7: A top view of the cell following a horizontal sectioning which exposes its hollow and fragmented interior. **(Color Plate 73, page 472)**

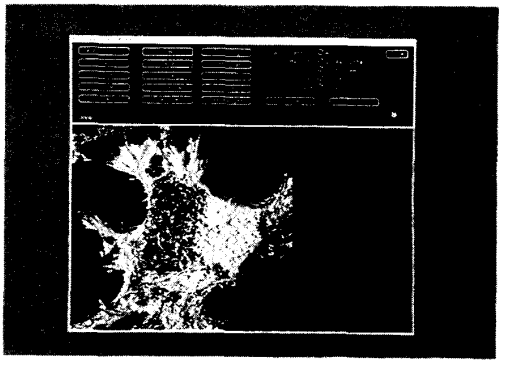

Figure 8: A bottom view of the cell demonstrating the organization of actin at the cell-substrate interface. **(Color Plate 74, page 472)**

the context sensitive method and to employ simple segmentation, context sensitive operators, and gradient calculation, which are all described below.

Segmentation into contexts is achieved by looking for changes in the depth function in order to identify context edges. For this purpose we define the *backward, forward,* and *central differences* (e.g., along the X axis) at the point (i, j) to be, respectively,

$$B_{i,j} = D_{i-1,j} - D_{i,j} \tag{2}$$

$$F_{i,j} = D_{i+1,j} - D_{i,j} \tag{3}$$

$$C_{i,j} = D_{i+1,j} - D_{i-1,j} = F_{i,j} - B_{i,j} \tag{4}$$

where $D_{i,j}$ is the depth value at the point (i,j).

A context edge is detected by observing one of two types of changes:

(i) A sharp change in the depth function indicating a possible C^0 discontinuity. This change is detected by observing if $|F_{i,j}| > \varepsilon^0$ for some predefined value ε^0.

(ii) A sharp change in the first derivative of the depth function indicating a possible C^1 discontinuity. This change is detected by observing if $|C_{i+1,j} - C_{i,j}| > \varepsilon^1$ for some predefined value ε^1.

The exact numerical value which defines the "sharpness" parameters ε^0 and ε^1 is application dependent. Dealing with geometrically defined scenes of moderate resolutions, we empirically discovered that the values 3 and 5, respectively, produce the best results in most cases.

In the prefiltering and postfiltering stages we use simple, context sensitive 3×3 weighted averaging filters. The final context-sensitive filtered value $\overline{V}_{i,j}$ at (i,j) is:

$$\overline{V}_{i,j} = \frac{\sum_{k\in N_x}\sum_{l\in N_y} P(\rho_{i,j}, \rho_{i+k,j+l})\,\omega_{k,l}\,V_{i+k,j+l}}{\sum_{k\in N_x}\sum_{l\in N_y} P(\rho_{i,j}, \rho_{i+k,j+l})\,\omega_{k,l}} \tag{5}$$

where:

$P(\rho_{i,j}, \rho_{r,s})$ is a predicate that returns *true* (1) if the pixels $\rho_{i,j}$ and $\rho_{r,s}$ belong to the same context, and *false* (0) otherwise;

N_x, N_y are the X and Y neighborhoods included in the window seen by the filter along the X and Y axes (e.g., in the case of a 3×5 filter, $N_x = \{0, \pm1, \pm2\}$, $N_y = \{0, \pm1\}$);

$\omega_{k,l}$ are the user-controllable filter weights where $k \in N_x$, $l \in N_y$ and $\sum_{k\in N_x}\sum_{l\in N_y} \omega_{k,l} = 1$; and

$V_{i,j}$ is the original data value at (i,j).

The gradient values used for shading are calculated by employing a variation of the central difference (Equation (4)) as an estimation of the surface inclination within the context. Since the computation must be context sensitive, forward or backward differences are used at the context boundaries. The gradient $G_{i,j}$ at (i,j) is calculated as follows:

$$G_{i,j} = \begin{cases} C_{i,j}/2 & \text{if } P(\rho_{i,j}, \rho_{i+1,j}) \text{ and } P(\rho_{i,j}, \rho_{i-1,j}) \\ F_{i,j} & \text{if } P(\rho_{i,j}, \rho_{i+1,j}) \\ B_{i,j} & \text{if } P(\rho_{i,j}, \rho_{i-1,j}) \\ 0 & \text{Otherwise} \end{cases} \tag{6}$$

Figure 8 shows an image shaded by the context sensitive method. We used the values 3 and 5 for the parameters ε^0 and ε^1, respectively.

Concluding Remarks

When a physician or a radiologist examines an image of an organ produced by volume rendering, he usually knows what to expect and how the organ should look because the real object is accessible and can be manipulated. Thus, it is relatively easy to tune the visualisation parameters for the production of optimal images. However, the cell biologist can only access the cell indirectly via a microscope. Moreover, the diverse morphologies of individual cell types and the multiple shapes a cell can assume during its life span make it extremely difficult to determine the quality and integrity of the rendering technique. The approach we took is based on providing a rich set of tools for volumetric exploration and rendering, which can be used by the biologist to gain a better understanding of the spatial relationship between sub-cellular structures in the volumetric scene. Figures 4-8 show the use of such tools as slicing, combining shading methods, changing of color palettes, positioning of the light source, and more.

Despite the inherent difficulties encountered when trying to visualize in 3D the actin cytoskeleton, we have demonstrated the feasibility of our visualization approach and provided for the first

time a 3D image of the actin cytoskeleton. This image can be further investigated by a variety of volume manipulation tools, provided by our BioCube environment. The significance of this achievement can be appreciated by remembering that cell biologists have thus far seen the cytoskeleton, as well as other cellular structures, only in the form shown in Figures 1-3. A comparison between Figures 1-3 and Figures 4-8 demonstrates the immense amount of information that becomes available to the biologist when using 3D volume visualization methods. This information represents an important step towards understanding the real structure of single cells.

BioCube is an environment that furnishes the tools for volumetric exploration of microscopic objects. Its implementation is based upon the functionalities provided by the Cube workstation [12], a general-purpose environment of basic tools for a variety of voxel-based applications, utilizing a 3D lattice of voxels to represent the volumetric objects. Like the Cube workstation, the BioCube environment supports different volumetric projection types (orthographic and arbitrary parallel projection of any sub-volume), voxel input, geometric model voxelization (e.g., [11]), transformation and manipulation [14], 3D interaction [15], image sectioning, cut planes, color and density segmentation, translucency, shading, and measurements.

The BioCube environment can also be supported by the Cube architecture [13], which is a special-purpose hardware for volume visualization. Based on the successful realization of reduced resolution prototypes, we are currently designing a full-scale 256^3 resolution VLSI prototype that will run, in real time, a wide range of volume visualization applications, and the BioCube environment in particular. Running the BioCube in hardware will equip the biologist with real-time interactive exploration tools, which are intrinsic features of the Cube architecture (e.g., viewing, slicing, translucencies, voxel operations, shading).

Some present acquisition technologies are capable of supporting close to real-time acquisition rates [9]. Confocal microscopy is constantly improving and is expected to support similar or better capabilities in the near future. Moreover, in some biological processes the rate of change is relatively slow, and thus acquisition rates required for optimal visualization are less than real time. The implementation of a system that will provide visualization of 4D data is confronted with major problems, such as data storage, compression, enhancement, manipulation time, and rendering. The field of 4D volume rendering is in its infancy and not much work has been published (e.g., [22, 23]). We do believe, however, that the coupling of a special-purpose volume rendering hardware (e.g., the Cube architecture machine) with newer generation confocal and digital video microscopy will allow the biologist to visualize and digitally manipulate three dimensional *in-vivo* processes.

Acknowledgments

This project has been supported by the National Science Foundation under grants MIP 8805130 and CDA 8947756, the National Institute of Health under grant GM 32776 (I.S.), and grants from Hughes Aircraft Company, Hewlett Packard, and Silicon Graphics. We thank Dr. P. R. Adams and Mr. B. J. Burbach of the Howard Hughes Medical Institute for the use of the confocal microscope, and Mr. S. Hongchi for his help in the BioCube system.

References

1. Agard, D. A., Hiraoka, Y., Shaw, P. and Sedat, J. W., "Fluorescence Microscopy in Three-Dimensions", *Methods in Cell Biology*, **30**, (1989), 353-377, Academic Press.

2. Artzy, E., Frieder, G. and Herman, G. T., "The Theory, Design, Implementation and Evaluation of a Three Dimensional Surface Detection Algorithm", *Computer Graphics and Image Processing*, **15**, 1 (January 1981), 1-24.

3. Cohen, D., Kaufman, A., Bakalash, R. and Bergman, S., "Real-Time Discrete Shading", *The Visual Computer*, **6**, 1 (February 1990), 16-27.

4. Fay, F. S., Fogarty, K. E. and Coggins, J. M., "Analysis of Molecular Distribution in Single Cells Using a Digital Imaging Microscope", in *Optical Methods in Cell Physiology*, P. DeWeer and B. M. Salzberg, (eds.), Wiley, 1986, 51-64.

5. Foley, J. D. and van Dam, A., *Fundamentals of Interactive Computer Graphics*, Addison-Wesley, Reading, MA, 1982.

6. Frieder, G., Gordon, D. and Reynolds, R. A., "Back-to-Front Display of Voxel-Based Objects", *IEEE Computer Graphics and Applications*, **5**, 1 (January 1985), 52-60.

7. Gordon, D. and Reynolds, R. A., "Image Space Shading of 3-Dimensional Objects", *Computer*

Vision, Graphics and Image Processing, **29**, (1985), 361-376.

8. Herman, G. T., Reynolds, R. A. and Udupa, J. K., "Computer Techniques for the Representation of 3D Data on a 2D Display", *SPIE*, **367**, (1982), 3-6.

9. Hiraoka, Y., Minden, J. S., Swedlow, J. R., Sedat, J. W. and Agard, D. A., "Focal Points for Chromosome Condensation and Decondensation Revealed by Three-Dimensional *in vivo* Time-Lapse Microscopy", *Nature*, **342**, (November 1989), 293-296.

10. Hoehne, K. H. and Bernstein, R., "Shading 3D-Images from CT Using Grey-Level Gradients", *IEEE Transactions on Medical Imaging*, **MI-5**, 1 (March 1986), 45-57.

11. Kaufman, A., "Efficient Algorithms for 3D Scan-Conversion of Parametric Curves, Surfaces, and Volumes", *Computer Graphics*, **21**, 4 (July 1987), 171-179.

12. Kaufman, A., "The CUBE Workstation - a 3D Voxel-Based Graphics Environment", *The Visual Computer*, **4**, 4 (October 1988), 210-221.

13. Kaufman, A. and Bakalash, R., "Memory and Processing Architecture for 3D Voxel-Based Imagery", *IEEE Computer Graphics and Applications*, **8**, 11 (November 1988), 10-23.

14. Kaufman, A., " "The *voxblt* Engine: A Voxel Frame Buffer Processor"", in *Advances in Graphics Hardware III*, A. A. M. Kuijk and W. Strasser, (eds.), Springer-Verlag, Berlin, 1989.

15. Kaufman, A., Yagel, R. and Bakalash, R., "Direct Interaction with a 3D Volumetric Environment", *Proceedings 1990 Symposium on Interactive 3D Graphics*, Snowbird, Utah, March 1990, 33-34.

16. Levoy, M., "Display of Surfaces from Volume Data", *IEEE Computer Graphics and Applications*, **8**, 5 (May 1988), 29-37.

17. Morgenthaler, D. G. and Rosenfeld, A., "Multidimensional Edge Detection by Hypersurface Fitting", *IEEE Transactions on Pattern Analysis and Machine Intelligence*, **PAMI-3**, 4 (July 1981), 482-486.

18. Pawley, J., in *The Handbook of Biological Confocal Microscopy, The Confocal Microscopy Workshop*, The Electron Microscopy Society of America, San Antonio, TX, August 1989.

19. Pettigrew, J., Roberts, D., Riddle, R., Udupa, J., Collier, D. and Ram, C., "Identification of an Anteriorly Displaced Meniscus in Vitro by Means of 3-D Image Reconstruction", *Oral Surgical Oral Medicine Oral Pathology*, **59**, (1985), 535-542.

20. Raya, S. P. and Udupa, J. K., "Shape-based Interpolation of Multidimensional Objects", *IEEE Transactions on Medical Imaging*, 1990. (To appear).

21. Rhodes, M. L., Kuo, Y. M., Rothman, S. L. G. and Woznick, C., "An Application of Computer graphics and Networks to Anatomic Model and Prosthesis Manufacturing", *IEEE Computer Graphics & Applications*, **7**, 2 (February 1987), 12-25.

22. Rossignac, J. R., "Considerations on the Interactive Rendering of Four-Dimensional Volumes", *Proceedings of the Chapel Hill Workshop on Volume Visualization*, Chapel Hill, NC, May 1989, 67-76.

23. Santek, D., Leslie, L., Goodman, B., Diak, G. and Callan, G., "4-D Techniques for Evaluation of Atmospheric Model Forecasts", *Proceedings Digital Image Processing and Visual Communications Technologies in Meteorology*, **846**, (October 1987), 75-77.

24. Sobierajski, L., Cohen, D., Kaufman, A. and Yagel, R., "Interactive Voxel-Based Surgical Planning System", Tech. Rep. 90.05.22, Computer Science, SUNY at Stony Brook, May 1990.

25. Spector, I., Shochet, N. R., Blasberger, D. and Kashman, Y., "Latrunculins - Novel Marine Macrolides that Disrupt Microfilament Organization and Affect Cell Growth: I. Comparison with Cytochalasin D", *Cell Motility and the Cytoskeleton*, **13**, (1989), 127-144.

26. Tuy, H. K. and Tuy, L. T., "Direct 2-D Display of 3-D Objects", *IEEE Computer Graphics & Applications*, **4**, 10 (November 1984), 29-33.

27. Van Zandt, W. and Argiro, V., "A New 'Inlook' on Life", *Unix Review*, **7**, 3 (1989), 52-57.

28. Vannier, M. W., Drebin, R. A. and Gayou, D. E., "Applications in Diagnosis and Reconstruction Methods for Generic Serial Sections", *Proceedings of NCGA'89 Conference*, **I**, (April 1989), 215-226.

29. Yagel, R., Cohen, D. and Kaufman, A., "Context Sensitive Normal Restoration for Volume Imaging", Tech. Rep. 90.05.15, Computer Science, SUNY at Stony Brook, May 1990.